

Testing of DLR C/C-SiC and C/C for HIFiRE 8 Scramjet Combustor

David E. Glass* and Diego P. Capriotti†
NASA Langley Research Center, Hampton, VA 23681 USA

Thomas Reimer‡ and Marius Kütemeyer§
Deutsches Zentrum für Luft- und Raumfahrt (DLR), Pfaffenwaldring 38-40, Stuttgart, Germany

and

Prof. Michael Smart**
The University of Queensland, Brisbane, Australia

Ceramic Matrix Composites (CMCs) have been proposed for use as lightweight hot structures in scramjet combustors. Previous studies have calculated significant weight savings by utilizing CMCs (active and passive) versus actively cooled metallic scramjet structures. Both a carbon/carbon (C/C) and a carbon/carbon-silicon carbide (C/C-SiC) material fabricated by DLR (Stuttgart, Germany) are being considered for use in a passively cooled combustor design for Hypersonic International Flight Research Experimentation (HIFiRE) 8, a joint Australia / Air Force Research Laboratory hypersonic flight program, expected to fly at Mach 7 for ~30 sec, at a dynamic pressure of 55 kPa. Flat panels of the DLR C/C and C/C-SiC materials were installed downstream of a hydrogen-fueled, dual-mode scramjet combustor and tested for several minutes at conditions simulating flight at Mach 5 and Mach 6. Gaseous hydrogen fuel was used to fuel the scramjet combustor. The test panels were instrumented with embedded Type K and Type S thermocouples. Zirconia felt insulation was used during some of the tests to reduce heat loss from the back surface and thus increase the heated surface temperature of the C/C-SiC panel ~177°C (350°F). The final C/C-SiC panel was tested for three cycles totaling over 135 sec at Mach 6 enthalpy. Slightly more erosion was observed on the C/C panel than the C/C-SiC panels, but both material systems demonstrated acceptable recession performance for the HIFiRE 8 flight.

Nomenclature

ER	=	Equivalence Ratio
$FUELIP$	=	Fuel Supply Pressure
M	=	Mach number
P	=	Pressure
P_0	=	total pressure
$PTOTAL1$	=	Facility Total Pressure
q_{dot}	=	heat flux
T	=	Temperature
T_t	=	Total temperature
T_w	=	Temperature at wall surface
x	=	distance from the facility nozzle exit plane (exit of the ramjet inlet)
ϕ_{H2}	=	equivalence ratio of injected hydrogen fuel

* Project Engineer, Structural Mechanics and Concepts Branch, MS 190, Associate Fellow

† Research Aerospace Engineer, Hypersonic Airbreathing Propulsion Branch, MS 168

‡ Research Engineer, Institute of Structures and Design, Member

§ Research Engineer, Institute of Structures and Design

** Professor and Chair of Hypersonic Propulsion, School of Mechanical and Mining Engineering, Senior Member

I. Introduction

THE Hypersonic International Flight Research Experimentation (HIFiRE) Program is a collaboration between the Defence Science & Technology Organisation (DSTO) of Australia and the United States Air Force through its Air Force Research Laboratory (AFRL). The primary objectives of the HIFiRE program are to investigate fundamental hypersonic phenomena and to develop and demonstrate component technologies that enable the sustained operation of aerospace systems within the atmosphere at speeds greater than Mach 5. The current manifest of the HIFiRE program includes nine flights yielding basic scientific data with analyses relevant to the design of future aerospace systems.

Completed flights in the HIFiRE program, such as HIFiRE 1¹, have produced significant data on high-speed boundary layer transition. The launch technology used in HIFiRE is based around the sounding rocket approach developed during the HyShot Program at The University of Queensland². Thus far, HIFiRE test technology has been used to test partially complete scramjet flowpaths that remain attached to the second stage booster. Furthermore, the trajectory for the tests has been ballistic, with the scramjet experiment conducted upon re-entry to the atmosphere at very high flight path angles. In contrast, the HIFiRE 8 vehicle, shown in Figure 1, is intended to cruise at Mach 7 under scramjet power for 30 sec at approximately zero flight path angle. The more severe thermal environment of HIFiRE 8 relative to earlier HIFiRE flights results in the need for advanced thermal management solutions.



Figure 1. Image of the HIFiRE 8 flight vehicle.

State-of-the-art scramjet combustors utilize actively cooled metallic structures. However, ceramic matrix composites (CMC), due to their high temperature capabilities, have the potential to provide a passive alternative for at least a portion of the flowpath. Due to the relatively short test time (~30 sec) and single use nature of the HIFiRE 8 flight, a scramjet combustor constructed using a passive CMC material is being considered. Toward this end, flat panels of the DLR carbon/carbon-silicon carbide (C/C-SiC) were tested in the NASA Langley Direct Connect Supersonic Combustion Test Facility (DCSCTF, see Reference 3) using the Durable Combustor Rig (DCR) test article. In addition to the C/C-SiC, the DLR carbon/carbon (C/C) material was also tested.

II. Test Facility and Test Article

Tests of the DLR test articles were conducted in the DCSCTF. The facility is located in a 16- by 16- by 52-foot (4.8768- by 4.8768- by 15.8496-meter) test cell within Building 1221D at the NASA Langley Research Center in Hampton, Virginia. The facility has historically been used to test ramjet and scramjet flow paths at stagnation enthalpies duplicating that of flight at Mach numbers between 3.5 and 7.5. The facility is of a direct-connect, or connected-pipe, configuration such that the entire facility test gas mass flow passes through the flow path model; the flow at the exit of the facility nozzle simulates the flow entering the isolator of a ramjet or scramjet in flight. The stagnation enthalpy necessary to simulate the flight Mach number for the test is achieved through hydrogen-air combustion with oxygen replenishment to obtain a test gas with the same oxygen mole or mass fraction as atmospheric air (0.2095 or 0.2314, respectively). A schematic of the DCSCTF is shown in Figure 2.

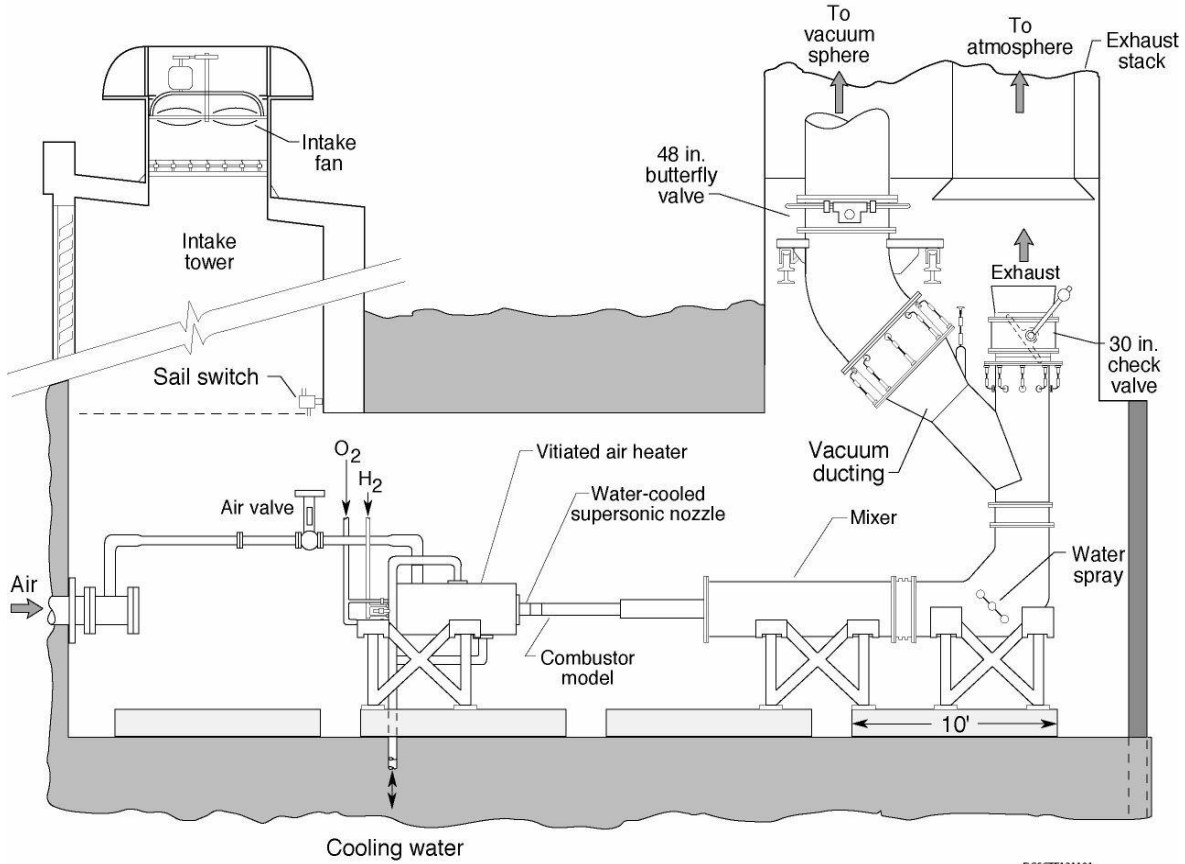


Figure 2. Schematic of the NASA Langley DCSCF.

The facility water-cooled combustion heater is supplied air from a 600-psig (4.1 MPa) high-pressure bottle field while hydrogen and oxygen are supplied from 2400-psig (16.5-MPa) tube trailers. Within the vitiated heater, oxygen is mixed with air before burning with hydrogen to increase the stagnation enthalpy of the flow. The vitiated air is then passed through a water-cooled supersonic nozzle, which is directly upstream of the test article. After passing through the test article, the flow enters the facility mixer where the exhaust test gas is cooled by water injection before eventually emptying into a 70-foot-diameter (21.3-m-diameter) vacuum sphere. Using two water-cooled facility nozzles, a Mach 2.1 and a Mach 2.65, the DCSCF can deliver flow fields that simulate the flow entering a ramjet or scramjet combustor at flight Mach numbers between 5 and 7. For the composite panel tests conducted, the Mach 2.1 nozzle was used at Mach 5 and 6 flight enthalpies. A summary of the nominal facility simulation points utilized is presented in Table 1. The hardware installed in the DCSCF for these tests comprised of existing hardware (Figure 3), and components fabricated especially for these tests. The existing hardware included a water cooled isolator and fuel injector block fabricated from thick walled copper, and an un-cooled divergent combustor also made of copper, but with a sprayed zirconia thermal barrier coating. The injector block contained a highly effective injection scheme that was able to inject and effectively mix and burn gaseous hydrogen fuel to simulate the conditions of a real combustor.

Table 1. Test conditions.

Simulated Flight Mach Number (at 1000 psf)	Facility Total Pressure (psia)	Facility Total Temperature (°R)	Facility Total Enthalpy (BTU/lb _m)	Facility Nozzle Exit Mach number	Facility Nozzle Exit Pressure (psia)	Facility Mass Flow Rate (lb _m /s)	Test gas water mole fraction
5	94.8	2103	574	2.12	10.0	8.08	12.7
6	91.4	2721	793	2.10	10.0	6.73	18.5

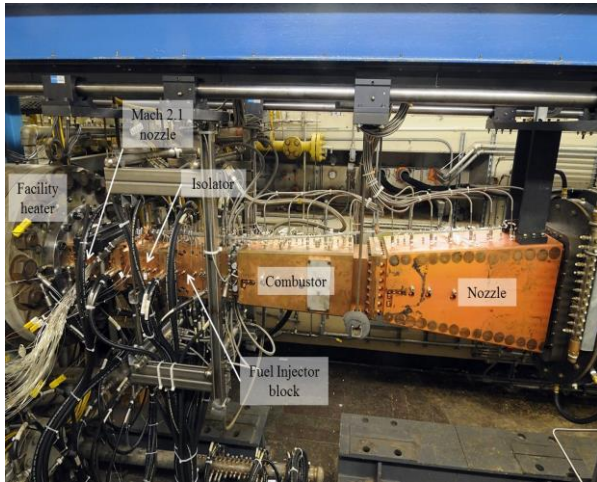


Figure 3. Photograph of DCR test hardware.

The new hardware consisted of a 6° divergent nozzle with the CMC panel installed on the top surface, and a steel plate on the bottom. The facility flowpath had a constant width of 5.21 inches (13.2 cm), and included pressure taps on both the top and bottom surfaces, except on the CMC panel. The CMC panel was instrumented with thermocouples (TCs) attached to the back side. Figure 4 shows an image of the nozzle exit, with a catch cone in place to collect the exhaust. Figure 5 shows a close-up view of the exhaust nozzle with the CMC plate installed as the top expanding surface.

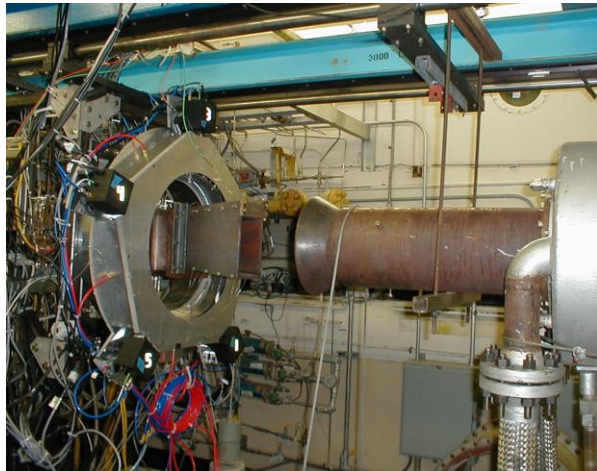


Figure 4. View of nozzle exit and exhaust duct installed in the DCSCF.

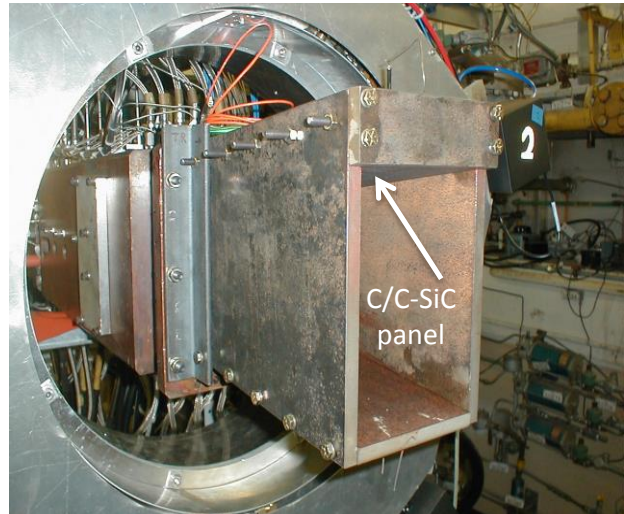


Figure 5. C/C-SiC panel mounted as the top wall of the 10-inch-long (25.4-cm-long), 6° diverging nozzle duct.

III. Characterization of the Test Flow Conditions

Using the inflow conditions, the measured wall pressures, the local duct area, the mass of fuel added, and estimates of the viscous drag and heat loss, the 1-D flow properties in the duct can be calculated. In the region where the CMC panel was installed ($x = 43$ inches (109.2 cm)), the total temperature of the flow was $T_t = 3900^\circ\text{R}$ (2167K), the static temperature was $T = 3200^\circ\text{R}$ (1778K), the static pressure was $P = 15$ psia (103 kPa) and the Mach number was $M = 1.35$. Based on a calculation of the facility boundary layer performed using the Van Driest II method, the heat load applied to a wall at $T_w = 540^\circ\text{R}$ (300K) in the region of the CMC panel was $q_{\text{dot}} (T_w = 300\text{K}) \sim 1.4 \text{ MW/m}^2$. Due to the higher total enthalpy, more fuel could be added in the combustor without disrupting the test, and typical fueling was at $\phi_{\text{H}_2} = 1.01$. At $x = 43$ inches (109.22 cm), the 1-D flow properties for these tests were $T_t = 4500^\circ\text{R}$ (2500K), $T = 3800^\circ\text{R}$ (2111K), $P = 14$ psia (96 kPa) and $M = 1.35$. The estimated heat load seen by the CMC panel in this case was estimated to be $q_{\text{dot}} (T_w = 300\text{K}) \sim 1.9 \text{ MW/m}^2$.

IV. Fabrication of DLR C/C-SiC and C/C Composite Panels

Ceramic matrix composites have been proposed for use as thermal protection materials and hot structures. At the Institute of Structures and Design of DLR in Stuttgart, a specific CMC variant, C/C-SiC has been developed consisting mainly of carbon fibers embedded in a silicon carbide matrix.⁴ The fabrication of C/C-SiC CMC composites at DLR is divided into three steps, as indicated in Figure 6. In the first step, a carbon fiber reinforced plastic (CFRP) component is produced, which can be performed in different ways. The preferred approach is resin transfer molding (RTM) or using autoclave technology, but warm pressing or filament winding are also acceptable processes. After the curing, the composites are tempered for 4 hours at 240°C (464°F) to complete the polymerization of the matrix. It is essential to use a resin (e.g., phenolic) with high carbon yield in this step to create a matrix with sufficient carbon content in the subsequent step.

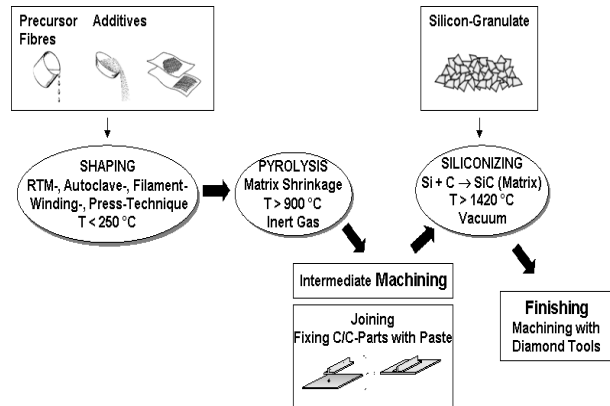


Figure 6. Schematic diagram of fabrication process.

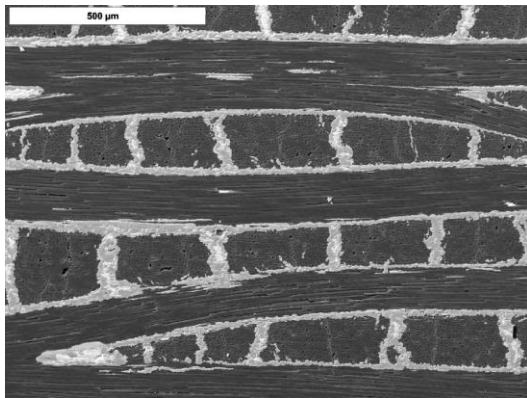


Figure 7. Typical microstructure of C/C-SiC: black color, fiber bundles with carbon matrix between fibers; medium grey, silicon carbide matrix; light grey/white, free silicon (scale bar is 500 μm).

In the second step, the CFRP composite is carbonized under inert atmosphere (nitrogen) at a temperature of 1650°C (3002°F) to convert the polymer matrix to amorphous carbon. The result is a C/C component. The pyrolysis results in a macroscopic shrinkage of about 10% mainly in thickness and a microscopic network of cracks within the C/C composite is formed. The fiber bundles remain practically intact.

The fabrication of the C/C plates is similar to that of the C/C-SiC plates through the first pyrolysis, the second step above. The result is a higher porosity and lower density C/C than a reinfiltreated C/C or siliconized C/C-SiC. In this case, however, the plates were reinfiltreated two more times with phenolic resin to increase the density and lower the porosity. In addition to the absence of Si and SiC, the C/C plates differ in the manufacturing of the initial CFRP. The C/C plates are warm pressed using short carbon fiber and phenolic resin, while the C/C-SiC plates are composed of carbon fiber weaves cured and infiltrated via autoclave.

In the third step, the C/C component is siliconized via melt infiltration. The component is placed into a coated graphite crucible and solid silicon is added as granulated pure metal. After heating to over 1420°C (2588°F) (melting of silicon), the porous C/C component fills with liquid silicon due to the capillary effect of the micro-cracks and the low viscosity of the molten silicon. In an exothermic reaction between the molten silicon and the carbon matrix, silicon carbide is formed along the micro cracks encapsulating the carbon fiber bundles. The siliconizing is carried out under vacuum at a temperature of 1650°C (3002°F). The resulting C/C-SiC composites contain three material phases. These are the carbon phase consisting of carbon fibers and residual carbon matrix, silicon carbide as the main matrix constituent, and a small share of unreacted free silicon, as shown in Figure 7. The typical thermal and mechanical properties of the C/C-SiC material are shown in Table 2.

Table 2. C/C-SiC properties.

Property	Direction	Value	Unit	Temperature
Density		1900	kg/m ³	
Young's Modulus	1	60	GPa	
	2	60	GPa	
	3	20	GPa	
Shear Modulus	12	8.8	GPa	
	23	8.9	GPa	
	13	8.8	GPa	
Poisson's ratio	12	0.032		
	23	0.032		
	13	0.032		
CTE	12	0.5E-06		20°C; 68°F
	12	2.5E-06		1600°C; 2912°F
Thermal Conductivity	1	18	W/mK	
	2	18	W/mK	
	3	9	W/mK	
Specific Heat		1000	J/kgK	20°C; 68°F
		1800	J/kgK	1600°C; 2912°F
Emissivity, total		0.75		20°C; 68°F
		0.8		1000°C; 1832°F
		0.85		1600°C; 2912°F

Plate material with fibers in 1-direction and 2-direction. No fibers in 3-direction (plate thickness)

V. Test Article Instrumentation

The C/C-SiC and C/C panels were instrumented at DLR prior to testing at NASA Langley. The panels were 254 mm (10 in.) long and 145 mm (5.7 in.) wide, with a thickness of 8 mm (0.315 in.) for the C/C-SiC panel and 10 mm (0.393 in.) for the C/C panel. The short edges were inclined slightly at an angle of 6° due to interface reasons with the DCSCF facility. The panels were machined on one side (the backside) to achieve the thickness. The other side remained in the as-fired condition as the plates come out of the processing. On the as-fired side (flow path side) only a few drops of excess silicon were removed. The reason for not machining both sides was that on the as-fired side there remains a thin scale of continuous SiC over the plate (which protects the panel fibers) whereas the machining exposes the carbon fibers to the hot combusting flow field. On the backside, grooves were machined for the installation of two thermocouples (Figure 8).

On each panel, two TCs were mounted. A curved groove was machined for each TC, as shown in Figure 9. The depth of the groove was 2 mm (0.079 in.). The TC tip was fixed in the groove with a graphite-based adhesive. Type K and Type S TCs of 1 mm (0.039 in.) diameter were installed. Table 3 gives the details about which TC type was installed in which panel.

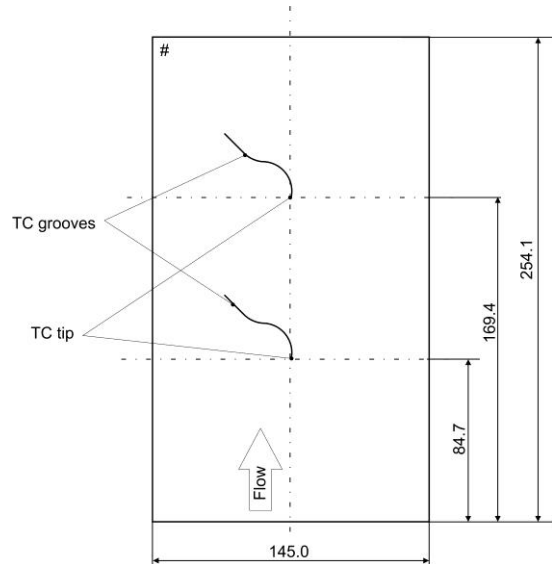


Figure 8. Location of the TCs as seen from backside (units in mm).

Table 3. Panels indicating type of TC installed.

Panel No.	Type K	Type S	Test load level
1	1	1	medium/ high
2	2	0	low
3	1	1	medium/high
4	1	1	spare

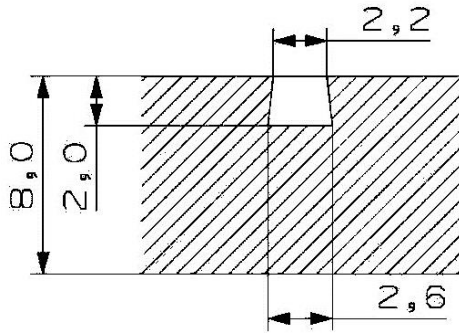


Figure 9. Cross section of TC groove (units in mm).

In order to provide support in addition to the graphite adhesive, the grooves were machined as dovetail grooves with an S-curve as detailed in the following cross section sketch. The TCs were installed on the symmetry axis at 84.7 mm (3.33 in.) and 169.4 mm (6.67 in.) from the edge, lengthwise (Figure 8). Figure 10 through Figure 12 illustrate the installation of the TCs.



Figure 10. Panel seen from machined side with TC grooves.

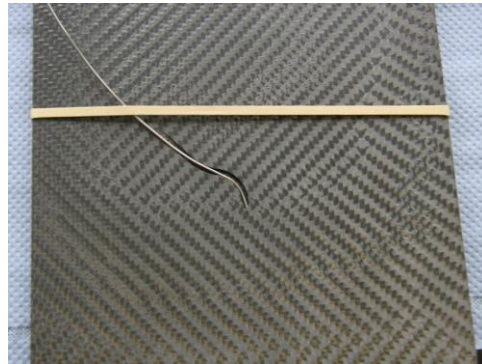


Figure 11. TC inserted into groove.



Figure 12. Graphite adhesive applied on TC tips.

VI. Test Results

The test matrix is shown in Table 4. Three C/C-SiC and one C/C panels were tested, with multiple tests per panel. The test hardware was allowed to cool down for approximately 20 minutes between tests. The facility run number is shown, followed by the simulated flight Mach number, either Mach 5 or 6. The actual (aerodynamic) Mach number of the flowfield within the DCR was ~Mach 2. As mentioned previously, two TC's were embedded in the panel from the back surface. In each of the panels tested, there was one Type K and one Type S TC installed. Shown in the table are the temperatures of the TC at the end of each test. The facility total temperature and pressure are also shown in the table, along with the equivalence ratio (ER) of the injected hydrogen fuel. Finally, the fuel-on time and the total test duration are shown.

Table 4. Test Matrix

Panel	Run No.	Simulated Flight Mach No.	Temperature at end of Test, °R		Temperature at end of Test, °C		P ₀ psia	T ₀		ER	Fuel-on Time [sec]	Total Test Duration [sec]
			Type K	Type S	Type K	Type S		°R	°C			
C/C HP635-7	68	5	859	858	204	204	96.1	2131	911		n/a	20
	69	5	1507	1450	564	532	96.1	2117	903	0.556	35	40
	70	5	1611	1548	622	587	95.9	2130	910	0.741	35	40
	71	6	1002	1031	284	300	89.4	2546	1141		n/a	20
	72	6	1878	1796	770	725	91.8	2611	1177	0.986	40	45
	73	6	1026	1015	297	291	88.8	2558	1148		n/a	20
	74	6	1987	1800	831	727	91.6	2594	1168	1.003	39	44
	75	6	2051	1835	866	746	90.8	2626	1186	1.023	39	44
C/C-SiC #4	52	5	1005	972	285	267	92	1939	804		n/a	20
	53	5	1248	1193	420	390	91.6	1957	814		n/a	40
	54	5	997	971	281	266	91.8	1989	832		n/a	20
	55	5	1214	1329	401	465	92.6	2020	849	0.53	14	20
	56	5	1044	1062	307	317	94.2	2035	857		n/a	20
	57	5	1737	1834	692	746	94.5	2070	877	0.58	32.5	38.5
	58	5	1076	1087	325	331	94.2	2070	877		n/a	20
	60	5	1010	999	288	282	94.6	2059	871		n/a	20
C/C-SiC #3	62	6	1281	1291	439	444	90.6	2624	1185		n/a	20
	63	6	1295	1319	446	460	90.7	2647	1197		n/a	20
	64	6	2025	2206	852	952	90.6	2648	1198	1.01	30	40
C/C-SiC #1	76	6	1382	1317	495	459	89.6	2591	1166		n/a	20
	77	6	2352	2515	1034	1124	91.9	2599	1171	1.009	39	44
	78	6	2342	2504	1028	1118	91.2	2639	1193	1.039	39.5	44.5
	79	6	2336	2462	1025	1095	91.9	2654	1201	1.047	39.5	44.5



Figure 13. Photograph of zirconia insulation on cool surface of test panel.



Figure 14. Photograph of scramjet exhaust during Run 79.

In an effort to increase the hot surface temperature on the final test panel (Runs 76–79), zirconia insulation was placed on the cool surface of the panel (backside). A photograph of the zirconia insulation on the test panel is shown in Figure 13. The insulation increased the hot surface temperature by ~177°C (350°F). A photograph of the scramjet exhaust during Run 79 (final test with C/C-SiC panel) is shown in Figure 14. Flow is left-to-right with the test panel on the upper surface of the fixture on the left hand side of the photograph.

A plot of the data from the two embedded TC's is shown in Figure 15 (for Run 79). The Type S TC reads a higher temperature, and was located upstream of the Type K TC. The facility total pressure (PTOTAL1) and fuel supply pressure (FUEL1P) are also shown on the figure. A post-test photograph of the test panel heated surface is also shown on the figure.

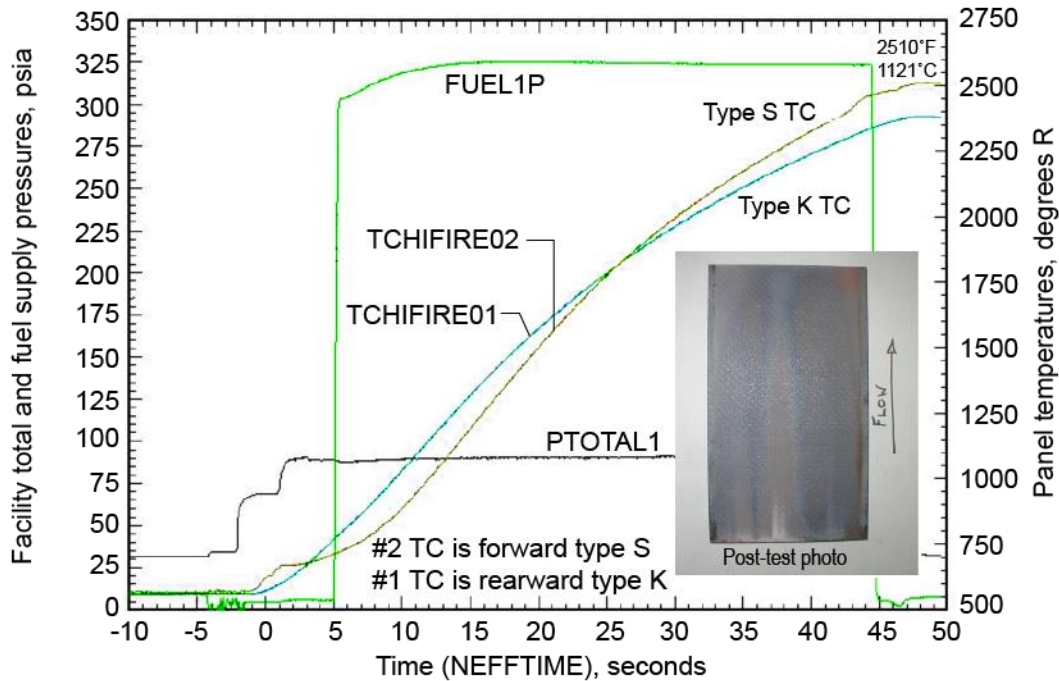


Figure 15. C/C-SiC panel test temperatures during Run 79.

After the final run, the test panel was removed from the carbon steel fixture. Figure 16 (a) shows a photograph of the fixture with the test panel removed. The red room-temperature vulcanizing (RTV) sealant (high-temperature silicone) can be seen in the photograph. Figure 16 (b) shows a close-up photograph of the corner region where the test panel was inserted into the groove on the right hand side. Seen in Figure 16 (b) is the melted carbon steel at the upstream edge of the fixture. Despite the high heating that the panel was subjected to during the last test and the melting of the steel sidewalls, the panel showed practically no damage, just a slight stain where the melted steel contacted the panel.

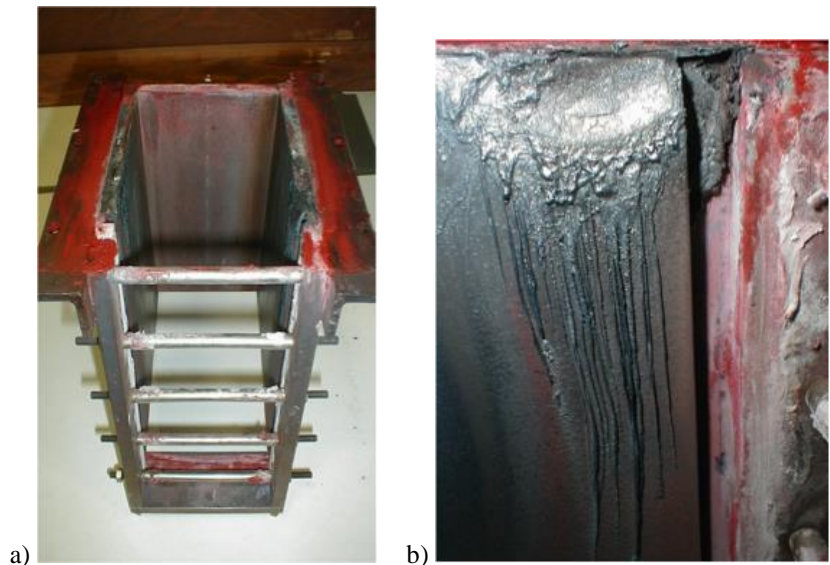


Figure 16. a) Photograph of test fixture after final test, and b) Close-up photograph after final test showing melted carbon steel fixture on test panel.

Figure 17 shows a photograph of both the hot and cool side of C/C-SiC panel #1 after the final test. As indicated by the recession measurements and the post-test photographs of the panel, the panel survived the series of tests with negligible deterioration.

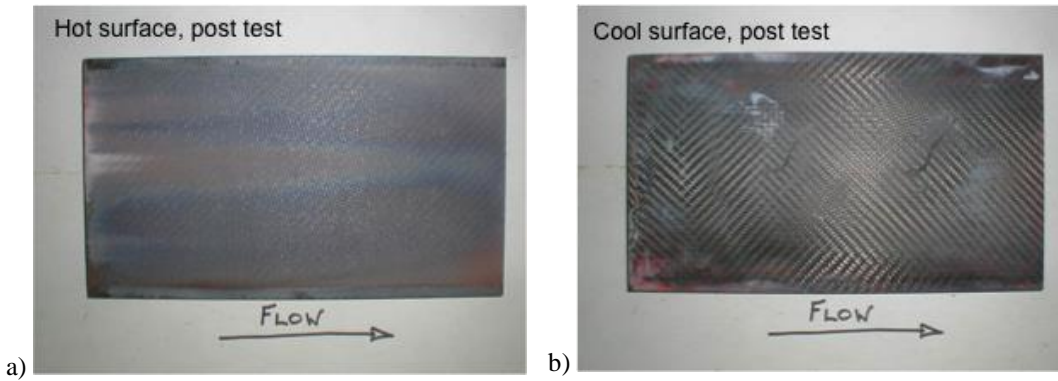


Figure 17. Photograph of a) hot surface and b) cool surface after Run 79.

Table 5 shows the pre- and post-test thickness measurements, taken prior to the first run with panel C/C-SiC #1 and taken again after the last run with C/C-SiC #1. Very little recession was measured on the test panels. Figure 18 shows the recession (change in thickness, Δt) at eight locations on the panel after Run 79. The largest recession was 0.051 mm (0.002 in.). Several locations have zero recession.

Table 5. Pre-and post-test thickness measurements for C/C-SiC panel #1.

	Thickness (mm) / Measurement location							
	1	2	3	4	5	6	7	8
Pre-test	8.026	8.052	8.052	8.103	8.306	8.280	8.052	8.052
Post-test	8.026	8.001	8.026	8.077	8.306	8.255	8.026	8.052

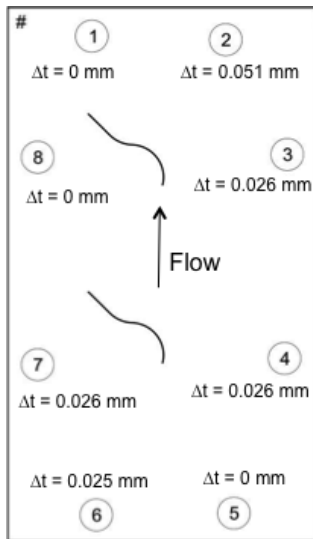


Figure 18. Recession measured after Run 79 for C/C-SiC panel #1.

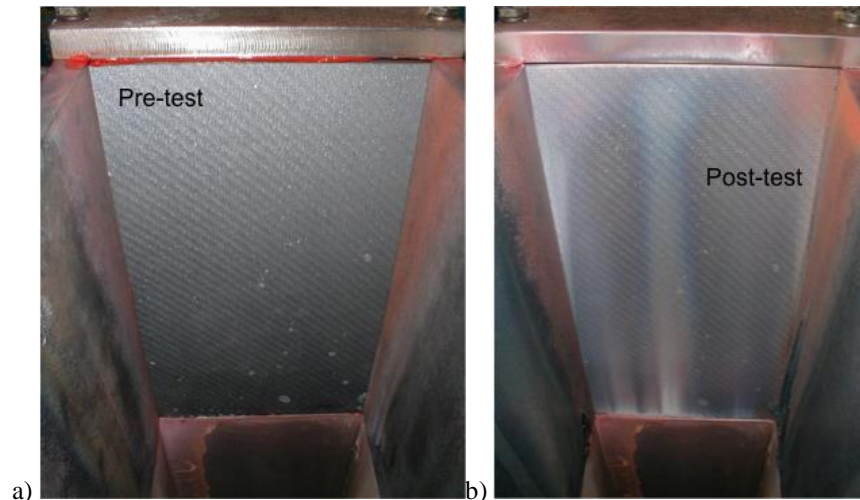


Figure 19. Pre- and post-test photograph of C/C-SiC panel installed in test fixture.

Photographs of the C/C-SiC panel 1 prior to testing and after the series of tests, are shown in Figure 19 (a). The discoloration shown in Figure 19 (b) is due to melting of the carbon steel support structure.

After the C/C-SiC panels were tested, a single C/C panel from DLR was also tested. A plot of the two embedded TC's is shown in Figure 20. The Type S TC reads a higher temperature, and was located upstream of the Type K TC. The facility total and fuel supply pressures are also shown on the figure. A photograph of the test panel post-test is also shown on the figure.

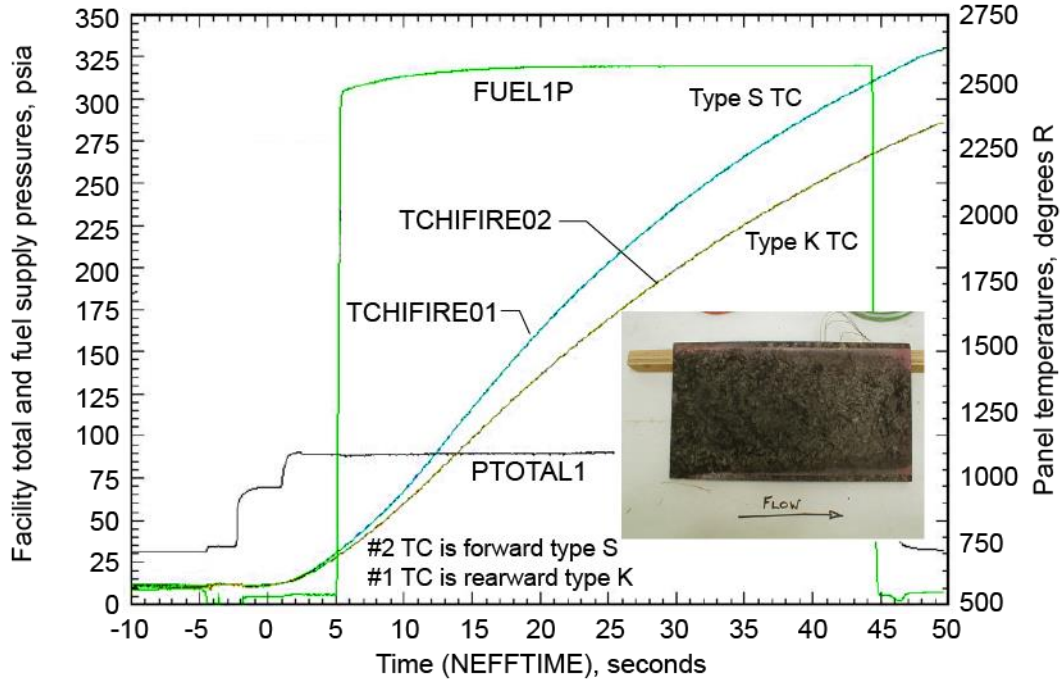


Figure 20. C/C panel test temperatures during Run 75.

A photograph of the C/C test panel posttest is shown in Figure 21. As shown in Table 4, the panel was tested for 100 seconds at Mach 5 conditions, and 193 seconds at Mach 6 conditions. The measured recession data are shown in Table 6, as well as graphically in Figure 22.

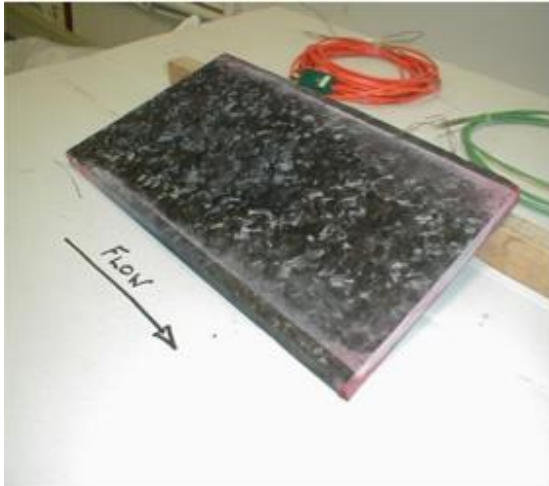


Figure 21. Post-test photograph of C/C panel HP635-7.

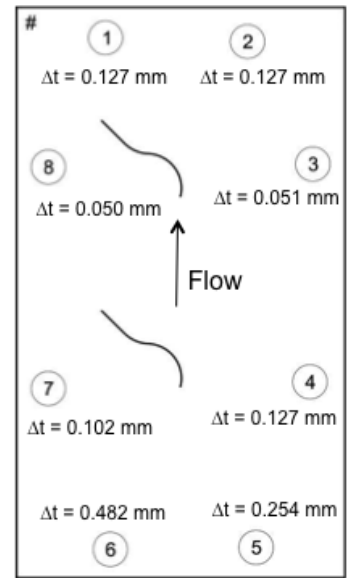


Figure 22. Recession measured after Run 75 on C/C panel HP635-7.

Table 6. Pre-and post-test thickness measurements for C/C panel HP635-7.

	Thickness (mm) / Measurement location							
	1	2	3	4	5	6	7	8
Pre-test	10.008	10.008	10.008	10.008	10.084	10.109	9.957	9.931
Post-test	9.881	9.881	9.957	9.881	9.830	9.627	9.855	9.881

VII. Post-test Investigation of C/C-SiC Panels

Several of the test panels were fabricated from C/C-SiC material as described previously. The surface that was to be exposed to the exhaust flow of the combustor was intentionally not machined in order not to remove the as-fabricated SiC layer that forms as the result of the material processing. The backside of the panels was machined and grooves for thermocouple installation were created (see Figure 10). Post-test investigations were performed with samples from all three tested C/C-SiC panels. Since the findings were consistent between the three panels, the process is described for panel #1 only.

A number of samples were prepared on the centerline of the panel and on a line that was 20 mm (0.79 in.) from the side edge of the panel. The panel was cut into 19 pieces, and each piece was numbered accordingly. The samples were prepared for investigations in the scanning electron microscope (SEM), i.e. they were embedded in a packing material and the surface to be investigated was ground and polished. For the investigations presented here, two samples from each panel were prepared. These were the cut-outs #5 and #17 from the centerline, as shown in Figure 23. Cut-out #5 was upstream on the panel closest to the combustor. Cut-out #17 was on the downstream end of the panel close to the nozzle exit.

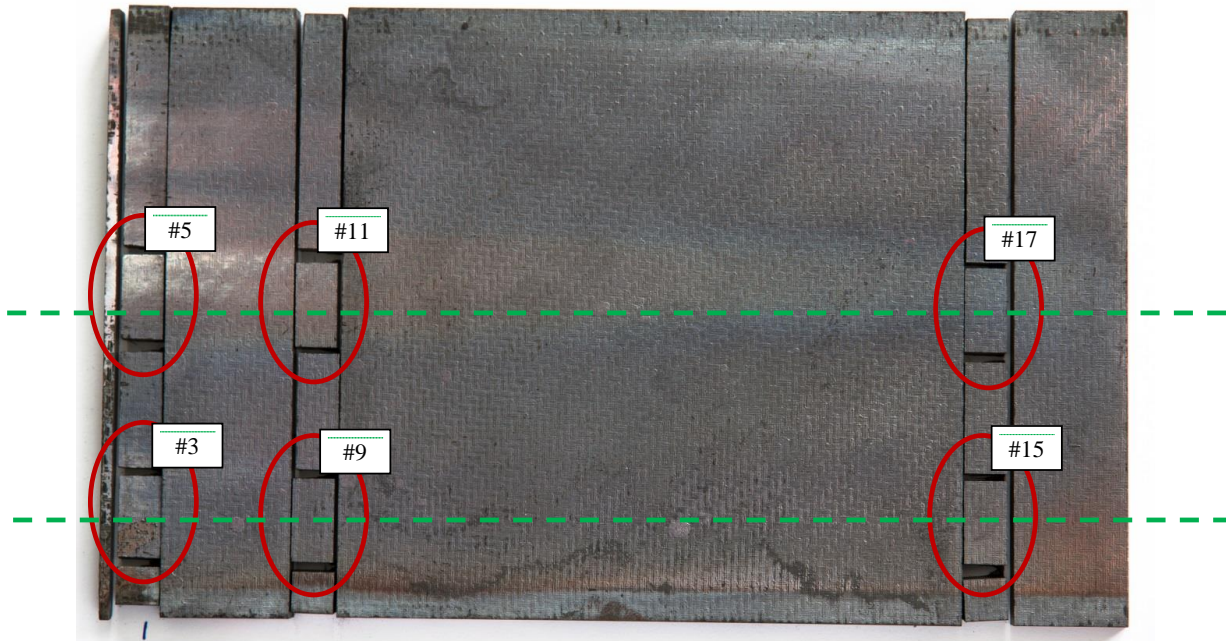


Figure 23. Panel 1 with cut pattern for the sample preparation.

Figure 24 shows an SEM image with the typical C/C-SiC microstructure. Carbon fiber bundles are separated by crack volumes that are filled with SiC at the boundaries and Si in the case when the width of the pore or crack is comparatively large. The surface of the sample is not flat because it was not machined, so the topology of the fiber textile is seen. The area on the top part of the image where numerous bright spots appear is the packing material used for embedding the sample.

There is no evidence of significant oxidation, which might have resulted in degraded fibers or matrix near the surface. What can be seen, is a thin bright layer on the surface that was identified as silicon dioxide (SiO_2 or silica) using electron diffraction spectroscopy (EDX) analysis.

The close-up of the detail highlighted in Figure 24 is shown in Figure 25. The different material phases can be distinguished very well. There is a fiber bundle with SiC on the surface. On the surface, above the SiC is a thin layer of silica $\sim 20 \mu\text{m}$ (0.0008 in.) thick. The SiO_2 layer on the surface does not have a constant thickness in every location over the sample. There are some spots where no SiO_2 layer can be found and there are locations with a thinner layer, but in general, there is a SiO_2 layer over most of the sample.

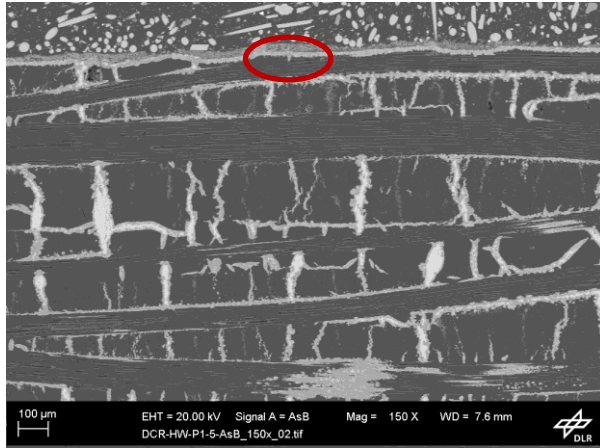


Figure 24. SEM image of sample #5 from panel 1. There is a thin layer on the surface that is identified as silica. Red circle indicates area that is shown in higher magnification in Figure 25.

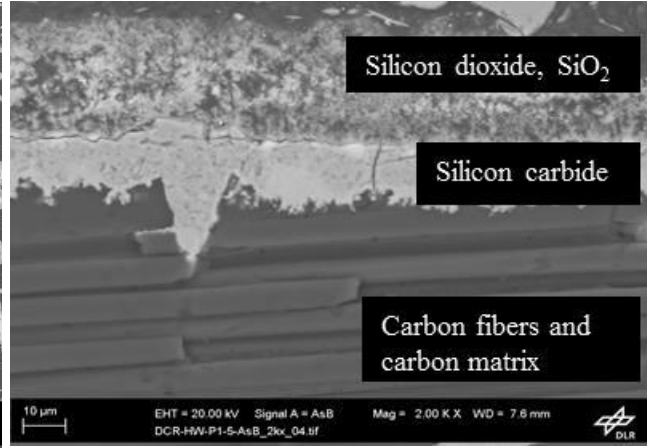


Figure 25. SEM image of the SiO₂ scale on top surface of the sample.

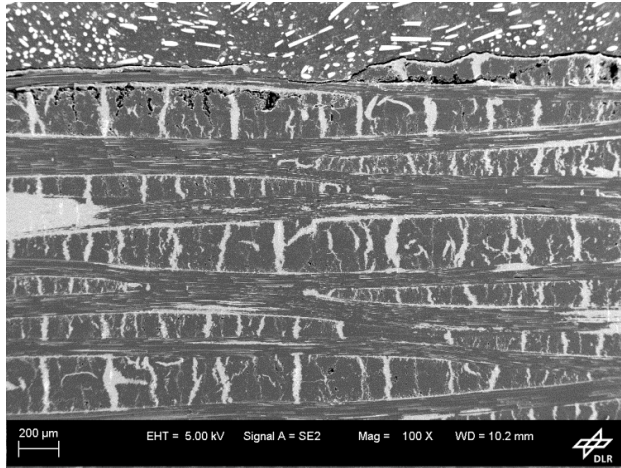


Figure 26. SEM overview image of sample #17 from panel 1, exposed surface is on the top.



Figure 27. Close-up SEM image showing some indication of matrix oxidation in the pore.

Figure 26 shows the surface of sample #17 from the end of the panel. There are a few cracks and pores in the two topmost layers. These could be the result of oxidation of the carbon since close-up images show signs of oxidation in the pores at fiber ends and on the matrix. However, the amount of pores was significantly smaller in other samples, so in part they can also be the result of sample preparation as there is a tendency of sample material to break out at the edges due to the relative softness of the surrounding packaging. Figure 27 shows a close-up SEM image showing some indication of matrix oxidation in the pore.

Note the clean-cut ends of most of the fibers as the result of the preparation. The circle indicates the region detailed in Figure 28.

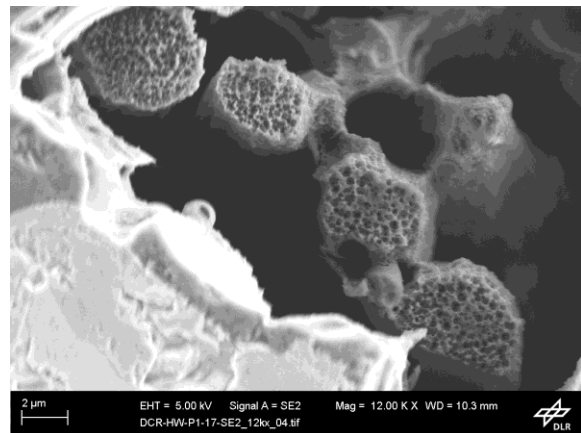


Figure 28. SEM image of fiber ends that have a rough cross-section, which is interpreted as the effect of oxidation.

VIII. Concluding Remarks

The DLR C/C and C/C-SiC materials were tested at NASA Langley Research Center in a high-enthalpy direct-connect test facility at conditions simulating flight at Mach 5 and Mach 6 for several minutes. The C/C-SiC survived the high-temperature scramjet combustor environment with very little erosion. The C/C material experienced slightly more erosion, but still only a small amount. SEM analysis of the tested panels indicated very little oxidation of the exposed surface. The HIFiRE 8 flight, for which the materials were tested, is planned for Mach 7 for ~ 30 sec. Due to the successful performance of the test panels, the DLR C/C-SiC material is being considered for use as a passive combustor on the HIFiRE 8 flight vehicle.

Acknowledgement

The technical effort reported herein was sponsored by the Hypersonic International Flight Research and Experimentation (HIFiRE) Program Office under an international collaboration between the Air Force Research Laboratory (AFRL) and the Australian Defence Science and Technology Organisation (DSTO). Specific Authority was secured under the terms and conditions of Project Arrangement (PA) AF-06-0046, and subject to terms and conditions secured under the joint US DoD-DoD Australia Memorandum of Understanding (MOU) for Co-operative and Collaborative Research, Development and Engineering.

References

- ¹Gosse, R., Kimmel, R., and Johnson, H. B., "Study of Boundary-Layer Transition on Hypersonic International Flight Research Experimentation 5," *Journal of Spacecraft and Rockets*, Vol. 51, 2014, pp 151-162.
- ²Smart, M. K., Hass, N. E. and Paull, A., "Flight Data Analysis of the HyShot 2 Flight Experiment," *AIAA Journal*, Vol. 44, No. 10, 2006, pp 2366-2375.
- ³Guy, R. W., Rogers, R. C., Puster, R. L., Rock, K. E., and Diskin, G. S., "The NASA Langley Scramjet Test Complex," (AIAA-96-3243), *AIAA, ASME, SAE, and ASEE, Joint Propulsion Conference and Exhibit*, 32nd, Lake Buena Vista, FL, July 1-3, 1996.
- ⁴Krenkel, W., *Ceramic Matrix Composites*, ISBN 978-3-527-31361-7 – Wiley-VCH, Weinheim, 2008.